Electronic Supplementary Information

A Full-spectrum-absorption from Nickel Sulphide Nanoparticles for Efficient NIR-II Window Photothermal Therapy

Ziyu Lei ,‡[a] Wenlong Zhang,‡[a] Bo Li,[d] Guoqiang Guan,[a] Xiaojuan Huang,[c] Xuan Peng,[a] Rujia Zou*[a] and Junqing Hu*[a, b]

[a] State Key Laboratory for Modification of Chemical Fibers and Polymer Materials, College of Materials Science and Engineering, Donghua University, Shanghai 201620, P.R. China.
[b] College of Health Science and Environmental Engineering, Shenzhen Technology University, Shenzhen 518118, China.
[c] Department of Oral and Maxillofacial-Head Neck Oncology, Shanghai Ninth People's Hospital, College of Stomatology, Shanghai Jiao Tong University School of Medicine; National Clinical Research Centre for Oral Diseases; Shanghai Key Laboratory of Stomatology&Shanghai Research Institute of Stomatology, Shanghai 200011, China.
[d] Department of Vascular Surgery, Shanghai Ninth People's Hospital, Shanghai Jiao Tong University School of Medicine, Shanghai 200011, China.

*Corresponding Author.

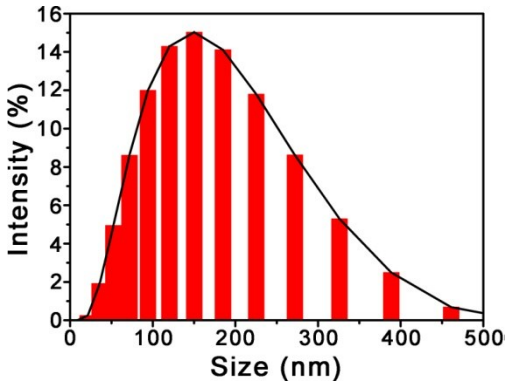

Figure S1. DLS pattern of as-prepared Ni_9S_8 NPs.

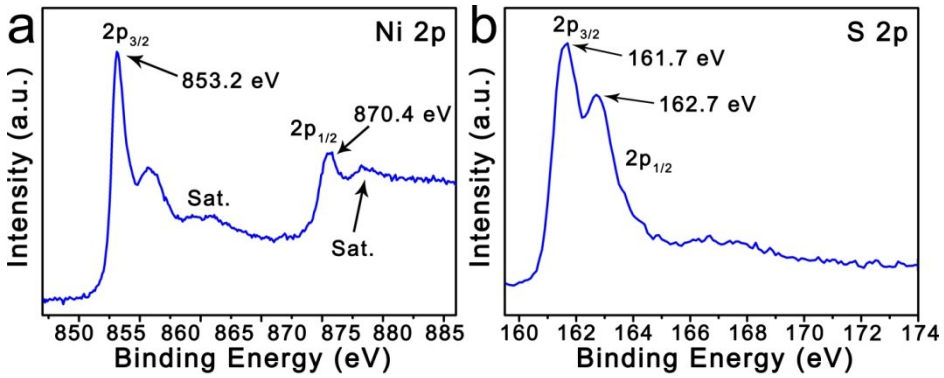

Figure S2. XPS patterns of (a) Ni 2p and (b) S 2p of the prepared Ni_9S_8 NPs.

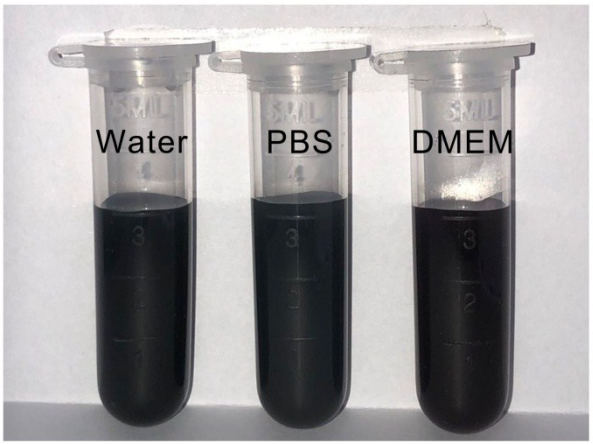

Figure S3. A camera picture of the Ni9S8 NPs dispersed in water (left), PBS (middle), and DMEM (right) for 7 days, showing the good dispersion of the NPs.

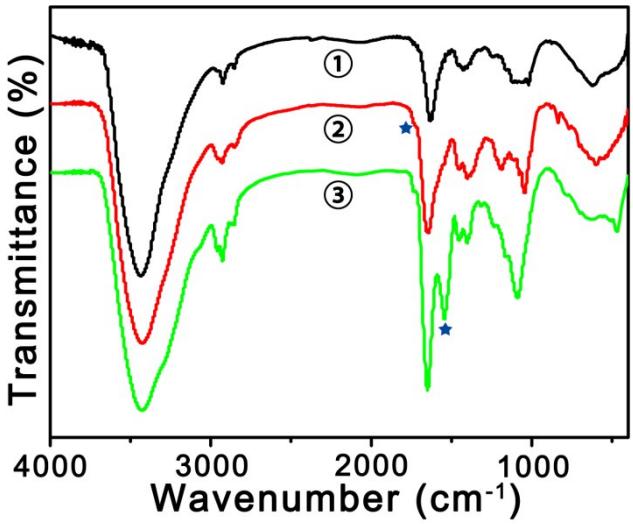

Figure S4. Fourier transform infrared (FTIR) spectra of the as prepared Ni_9S_8 NPs and other solutions: ①Ni_9S_8 NPs, ②Ni_9S_8 NPs-polymer and ③Ni_9S_8 NPs-polymer@BSA.

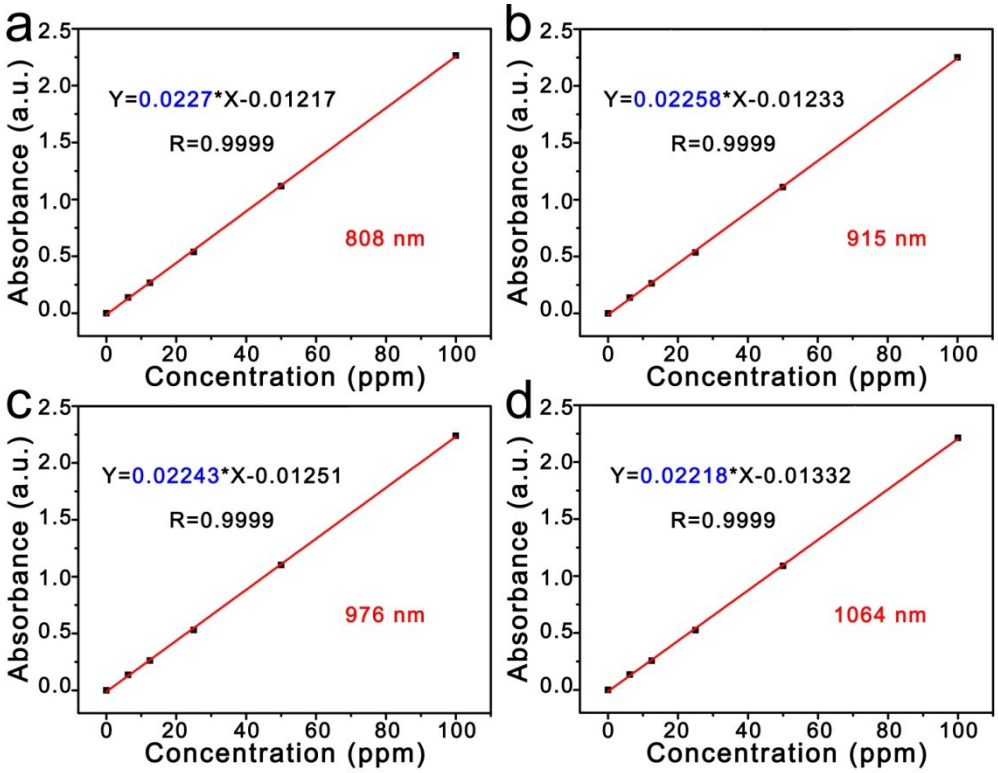

Figure S5. (a-d) Plots of linear fitting absorbance at 808, 915, 976 and 1064 nm versus concentrations of the Ni_9S_8 NPs' dispersions.

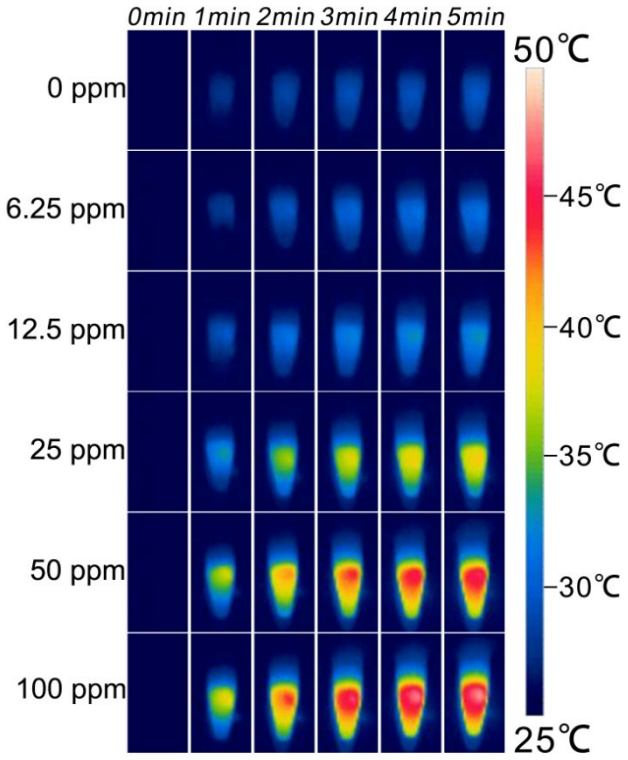

Figure S6. IR thermal images of the Ni_9S_8 NPs' dispersions with different concentrations upon 1064 nm laser irradiation at a power density of 0.7 W cm^{-2}.

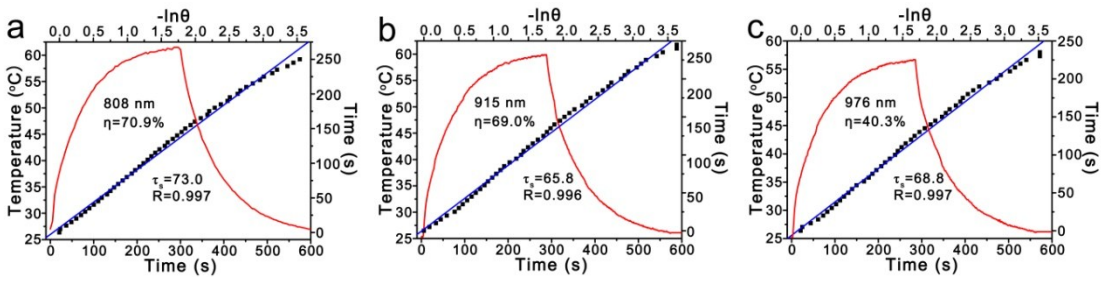

Figure S7. (a-c) Photothermal effect of the Ni_9S_8 NPs' dispersion upon being irradiated by 808, 915 and 976 nm laser at a power density of 0.7 W/cm^2. By applying the linear time data from the cooling period versus negative natural logarithm of driving force temperature, time constant (τs) for heat transfer from the system are determined to be 73.0, 65.8 and 68.8 s, respectively.

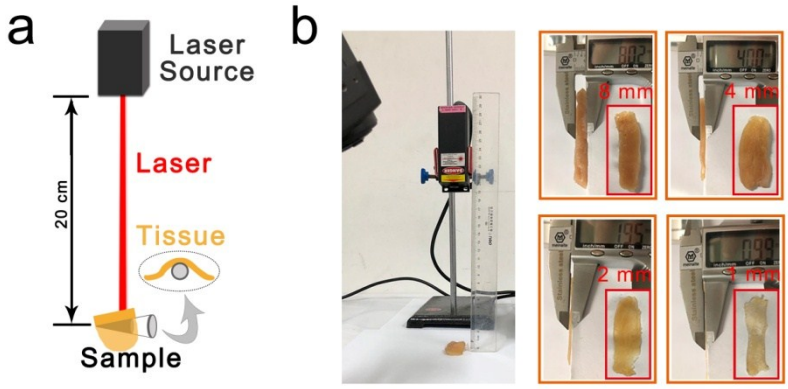

Figure S8. (a) Schematic diagram and (b) equipment for the photo-thermal temperature elevation of the chicken breast tissues with different thickness (1, 2, 4 and 8 mm) from the Ni_9S_8 NPs' dispersions irradiated by the NIR lasers (1 W cm^{-2}, 100 ppm).

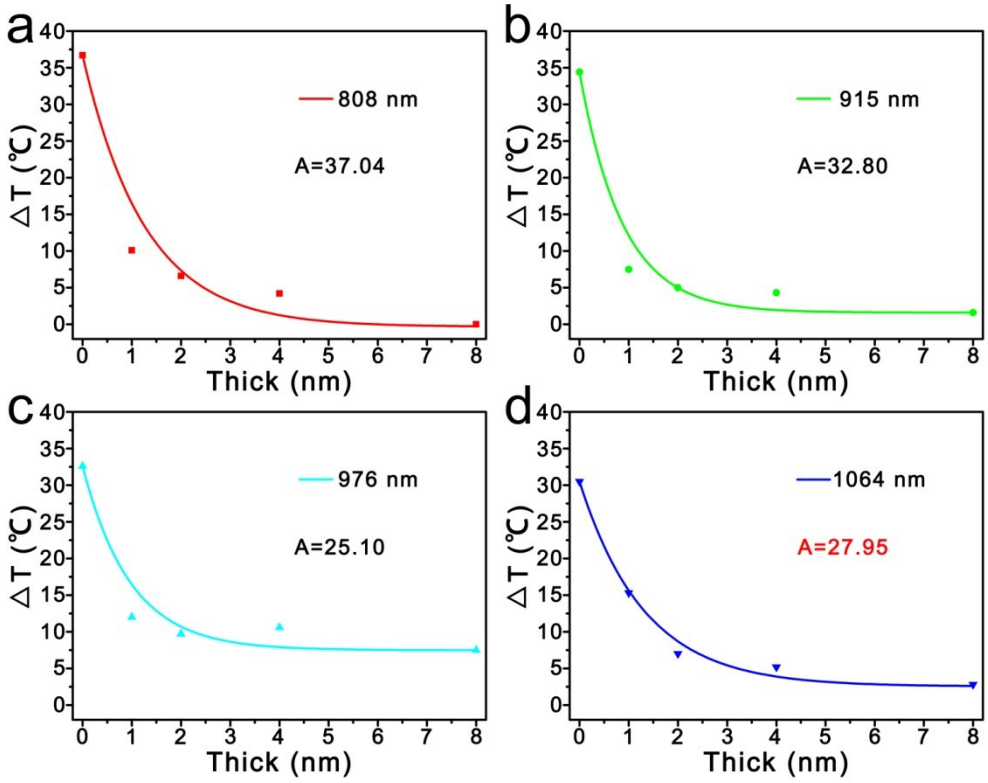

Figure S9. (a-d) Fitted exponential decay of temperature changes of the Ni_9S_8 NPs' solution covered by the chicken breast tissue with different depth upon the laser irradiation (at power density of 1W cm^{-2}) with different wavelength.

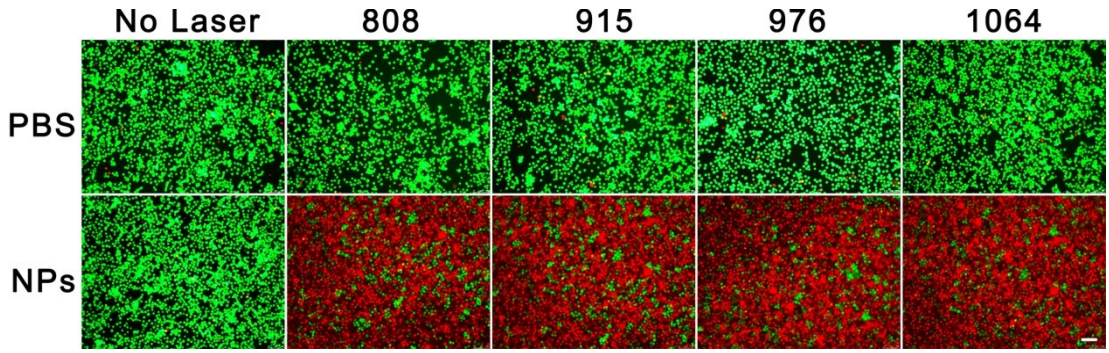

Figure S10. Fluorescence images of HeLa cells after various treatments, as labelled. The cells were co-stained with calcein AM (green, living cells) and propidium iodide (red, dead cells). The laser power densities were the MPE of the 808, 915, 976 and 1064 nm lasers, respectively. The scale bar is 100 μm.

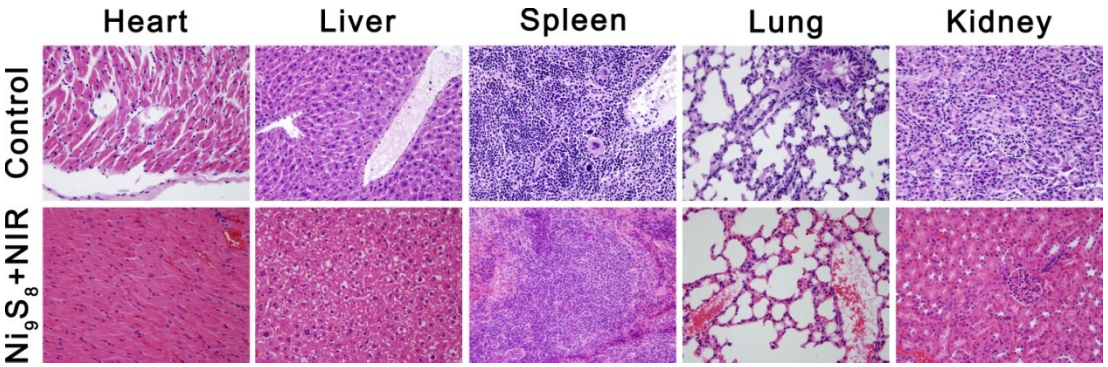

Figure S11. Major organs from untreated healthy mice as well as HeLa tumor-bearing mice 20 days after PTT by Ni_9S_8 NPs.

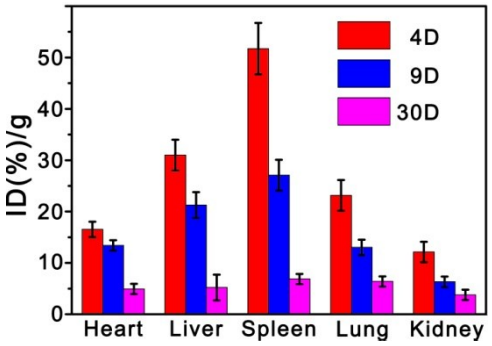

Figure S12. The biodistribution of Ni in main organs (i.e., heart, liver, spleen, lung, and kidney) at the 4, 9, 30 day after i.v. injection with the Ni_9S_8 NP aqueous dispersions (1000 ppm, 100 μL).